01,05,08

A RHEED study of the initial stages of Mn_5Ge_3 epitaxial growth on Si(111)

© I.A. Yakovlev, A.V. Lukyanenko, A.S. Tarasov, S.N. Varnakov

Kirensky Institute of Physics, Federal Research Center KSC SB, Russian Academy of Sciences, Krasnoyarsk, Russia

E-mail: yia@iph.krasn.ru

Received October 24, 2024
Revised December 14, 2024
Accepted December 15, 2024

The results of the crystal structure investigation of the interface layer and surface formed during the Mn_5Ge_3 thin film growth on silicon are presented in this paper. The dynamics of phase composition changes in the film at the initial stages of Mn_5Ge_3 growth on Si(111) 7×7 at 390 °C was studied by the reflected high-energy electron diffraction method. The diffraction data were analyzed by combining experimental patterns and calculated electron diffraction patterns for the expected phases, taking into account the data from the equilibrium phase diagrams. It was found that during the deposition of the first 0.5 nm, the formation of MnSi silicide predominates, then Mn_5Ge_3 begins to form together with MnSi at a film thickness of 2.5 nm. The single-phase Mn_5Ge_3 film begins to grow only at a thickness of more than 10 nm. Using atomic force microscopy, it was shown that when maintaining the stoichiometric ratio of Mn and Ge flows, during further growth on a silicon substrate without a buffer layer, a layer-by-layer plus island growth mode of the Stranski–Krastanov is realized.

Keywords: manganese germanide, manganese silicide, thin films, electron diffraction, ferromagnets, molecular beam epitaxy, spintronics.

DOI: 10.61011/PSS.2025.01.60579.276

1. Introduction

The creation of new materials and technologies that will allow the development of devices with lower energy consumption or with new functions is an urgent task of the scientific community. The transition to spintronic devices that use the degrees of freedom of electron spins, as well as their transport through semiconductor layers, is one of the most important areas of scientific research, the development of which will increase the speed of RAM and expand the possibilities of data storage, transmission and processing [1–5].

A solid solution of Mn_5Ge_3 is one of the promising materials [6–10] for solving semiconductor spintronics problems. It is a ferromagnetic metal with a Curie temperature of 296 K, which can be increased by doping with carbon [11], iron [12] or antimony [13]. In addition, it has a high spin polarization, and the effects of spin injection and detection into a semiconductor have already been demonstrated for it [14].

Mn_5Ge_3 films are most often synthesized on Ge substrates [15,16], since the thermodynamics of the Mn−Ge system favors this process, i. e. the enthalpy of formation is low compared to other compounds in the phase diagram of Mn−Ge [17]. This is also facilitated by the low lattice mismatch. GaAs(001) [18,19] and GaSb(001) [19] substrates are less commonly used. However, synthesis on Si(111) substrates is complicated due to a significant lattice mismatch (8%), as well as the formation of different manganese silicide phases. At the same time, it is necessary to synthesize promising ferromagnetic films on silicon substrates for combining the silicon industry capabilities and the spintronics potential. A special control of the material layers growth process with high crystalline quality and correct stoichiometry is required for the implementation of devices with high efficiency of spin injection and the further production of high-performance spintronic devices. It is important to study the growth process to obtain the necessary film properties since the structure and magnetic characteristics of Mn_5Ge_3 films can be significantly influenced by the type [19] and orientation [18] of single crystal substrates, the deposition temperature [20], annealing conditions [21] and the buffer layer thickness [22].

We previously studied the epitaxial films growth of Mn_5Ge_3 on Si(111) with different buffer layers thicknesses and stoichiometry [23–25]. In these investigations it was found that additional crystallographic orientations of Mn_5Ge_3, cubic phases of manganese germanides can be formed at the interface and silicon substitution can take place as well. In this paper an attempt to determine the interface layer composition was made. For this reason the investigation of initial stages growth of Mn_5Ge_3 on Si(111) were carried out.

2. Synthesis technique

Mn_5Ge_3 film was synthesized by molecular beam epitaxy (MBE) with simultaneous deposition of Mn (rate 0.35 nm/min) and Ge (rate 0.32 nm/min) from thermal effusion sources at a stoichiometric atomic ratio of Mn_5Ge_3 on Si(111)7×7 at 390°C in ultra-high vacuum MBE „Angara“ system optimized for the synthesis of silicides and

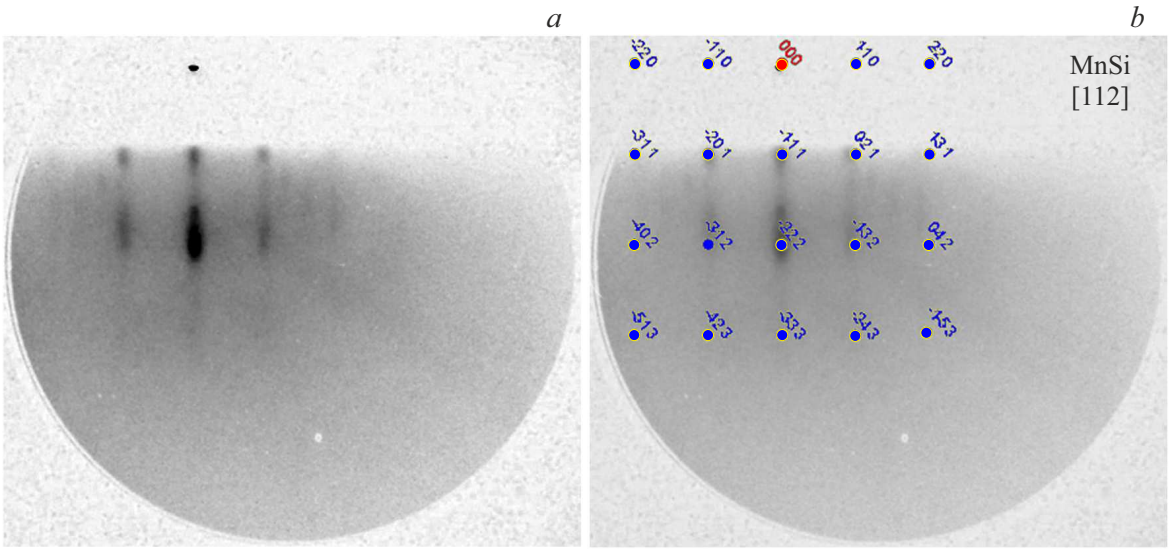

Figure 1. RHEED patterns from a 0.5 nm thick layer measured in the $[11\text{-}2]_{Si(111)}$ electron beam incidence direction: *a* — experimental pattern; *b* — pattern overlapping with the calculated pattern for MnSi in the $[112]_{MnSi}$ zone axis direction.

transition metal germanides [26–28]. The film thickness was 30 nm. The film formation process was controlled *in situ* by the reflection high-energy electron diffraction method (RHEED). The RHEED data were analyzed by combining experimental and calculated patterns for a given material. Theoretical electron diffraction pattern were calculated according to the kinetic diffraction theory with programs for cubic crystals [29] and hexagonal crystals.

3. Experimental results and discussion

Figure 1, *a* shows a RHEED pattern in the process of Mn and Ge co-deposition; only one grid of reflexes is clearly observed on it at an effective layer thickness of about 0.5 nm. The observed reflexes are well described by the cubic structure *c*P8 ($a = 0.45$ nm), which corresponds to manganese monosilicide MnSi (Figure 1, *b*).

There is no signal from germanium-containing compounds. It can be concluded from the analysis of the phase diagrams of Mn–Si, Mn–Ge, Si–Ge [30] that MnSi is formed at the initial stage, but germanium, to a greater extent, is used for the formation of a solid SiGe solution (not identified by RHEED). New groups of point reflexes appear in case of film deposition with a thickness in the range of 2–7 nm (Figure 2, *a*).

The dominant point grid of reflexes is matched with the structure Mn_5Ge_3 (*h*P16, $a = 0.71$ nm, $c = 0.50$ nm) (the points in Figure 2, *b*). Reflexes from MnSi are also poorly distinguishable (Figure 2, *b*). The same diffraction pattern also shows a group of point reflections (arrows in Figure 2, *b*) matched by a hexagonal lattice with parameters $a = 0.85$ nm and $c = 0.50$ nm, which do not correspond to any of the identified compounds among the compositions Mn–Si, Mn–Ge, Ge–Si. The point reflexes transform into streaks upon further deposition at a thickness of more than 10 nm (Figure 3), which indicates the transition of the film growth type from island to layer-island with large atomic terraces [31].

The analysis of diffraction data for over 10 nm films shows the formation of only one phase — Mn_5Ge_3. The calculated electron diffraction pattern for Mn_5Ge_3 with a hexagonal lattice constructed in the zone axis direction in a hexagonal crystal $[10.0]_{Mn_5Ge_3}$ is superimposed on the experimental RHEED pattern in Figure 3, *a* — a complete overlap of reflexes is observed. An additional diffraction pattern was measured in the $[110]_{Si(111)}$ incident electron beam direction to more accurately confirm the growth of only the specified compound, and an electron diffraction pattern was also calculated for it in the $[11.0]_{Mn_5Ge_3}$ zone axis direction. A complete overlap of patterns is also observed.

After reaching a film thickness of ~ 30 nm growth was stopped and *ex situ* studies of the morphology of the resulting film were performed by atomic force microscopy (AFM). AFM makes it possible to measure the relief of thin films with high accuracy and analyze morphological parameters. Figure 4 shows scans of the surface topology obtained in the semi-contact scanning mode of samples of Mn_5Ge_3 thin films directly on Si(111) silicon (Figure 4, *a*) and grown on Si(111) using a buffer layer (Figure 4, *b*), which was additionally formed at the initial stage of growth to compensate for the mismatch of the film and substrate lattices. This approach was previously described in detail in Ref. [26]. It is illustrative to use such a statistical tool as the two-dimensional autocorrelation function (ACF) for the comparison of the morphological parameters of the obtained thin films which shows the characteristic spatial frequencies of the surfaces. This approach has proven itself well for estimating the anisotropy of the surface films roughness [32].

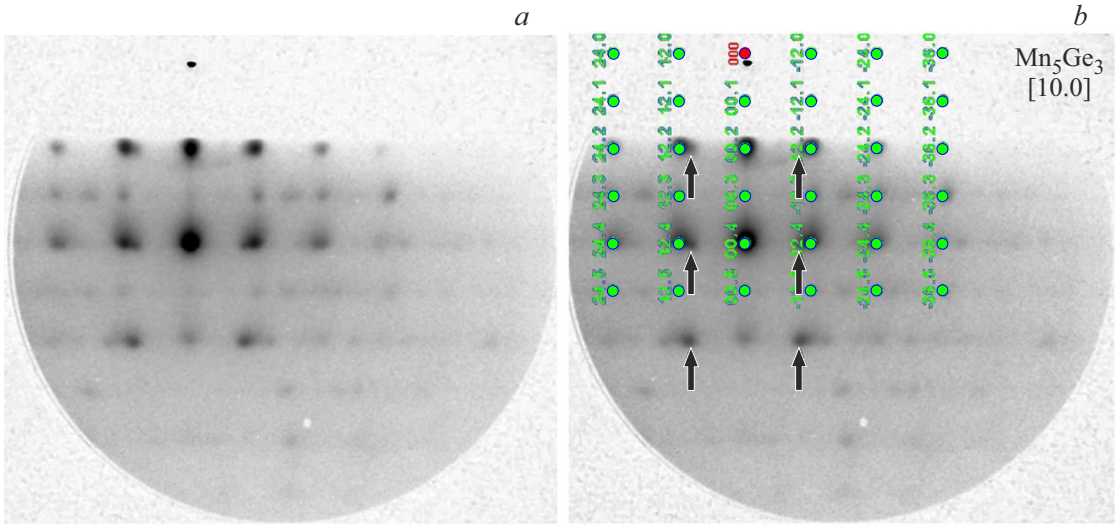

Figure 2. RHEED patterns from a 7.0 nm thick layer, acquired in the direction of the zone axis $[11\text{-}2]_{Si}$: *a* — experimental; *b* — combined with the calculated pattern for Mn_5Ge_3 in the $[11.0]_{Mn_5Ge_3}$ zone axis direction — points; reflexes from a hexagonal structure of unknown composition on the same axis (arrows). Green numbers — Miller indices of the crystallographic planes, which correspond to the presented reflexes on the calculated electronogram.

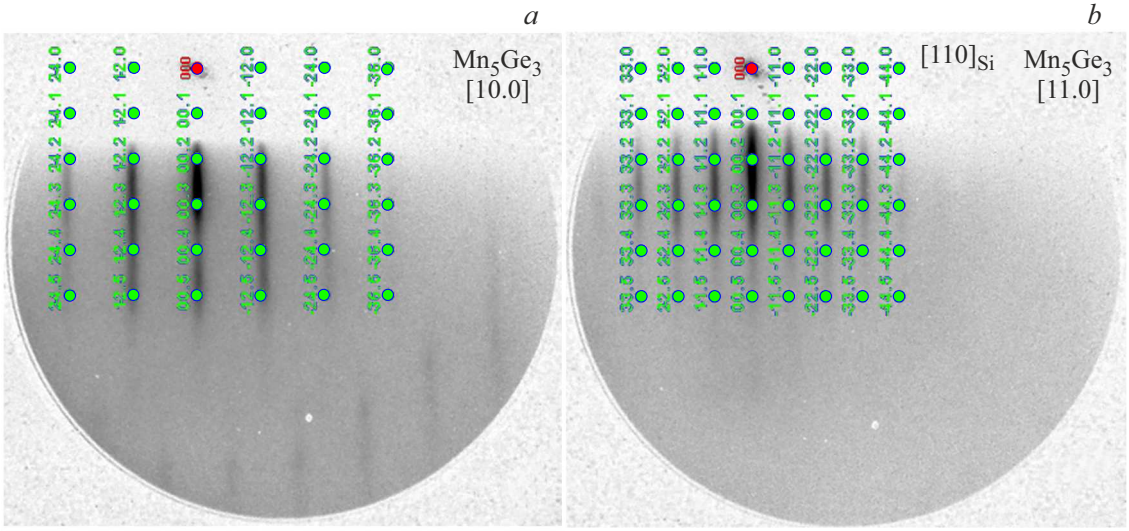

Figure 3. Experimental RHEED patterns from Mn_5Ge_3 film with a thickness of 30 nm and superimposed calculated electron diffraction patterns for Mn_5Ge_3 measured in the direction of the electron beam incidence: *a* — $[11\text{-}2]_{Si(111)}$; *b* — $[110]_{Si(111)}$.

This function can be calculated as a set of values for discrete AFM data

$$G(m,n) = \frac{1}{(N-n)(M-m)} \sum_{l=1}^{N-n} \sum_{k=1}^{M-m} z_{k+m,l+n} z_{k,l},$$

where z — the values of the bump height, N and M — the number of rows and columns of the data field; $M = \tau_x/\Delta x$, $N = \tau_y/\Delta y$, Δx and Δy — sampling intervals, with $\tau_x = x_1 - x_2$ and $\tau_y = y_1 - y_2$ for points (x_1, y_1), (x_2, y_2).

The autocorrelation length S_{al} is the shortest distance at which the ACF drops to values below the selected threshold of 0.02 (the threshold is marked with a mask in Figure 4, *d*). The corresponding cross-section charts of the two-dimensional ACF show profiles for the directions of the fastest (black cross-section lines) and slowest attenuation (red), respectively.

Based on the statistical data of the AFM, it can be concluded that the Stranski-Krastanov (island-plus-layer) growth mechanism is realized in the case of the growth of a manganese germanide film on silicon (Figure 4, *a*). This can be clearly shown by comparing the ACF length for both film samples. It can be seen in Figure 4, *d* (#a) that the two-dimensional ACF is practically isotropic and

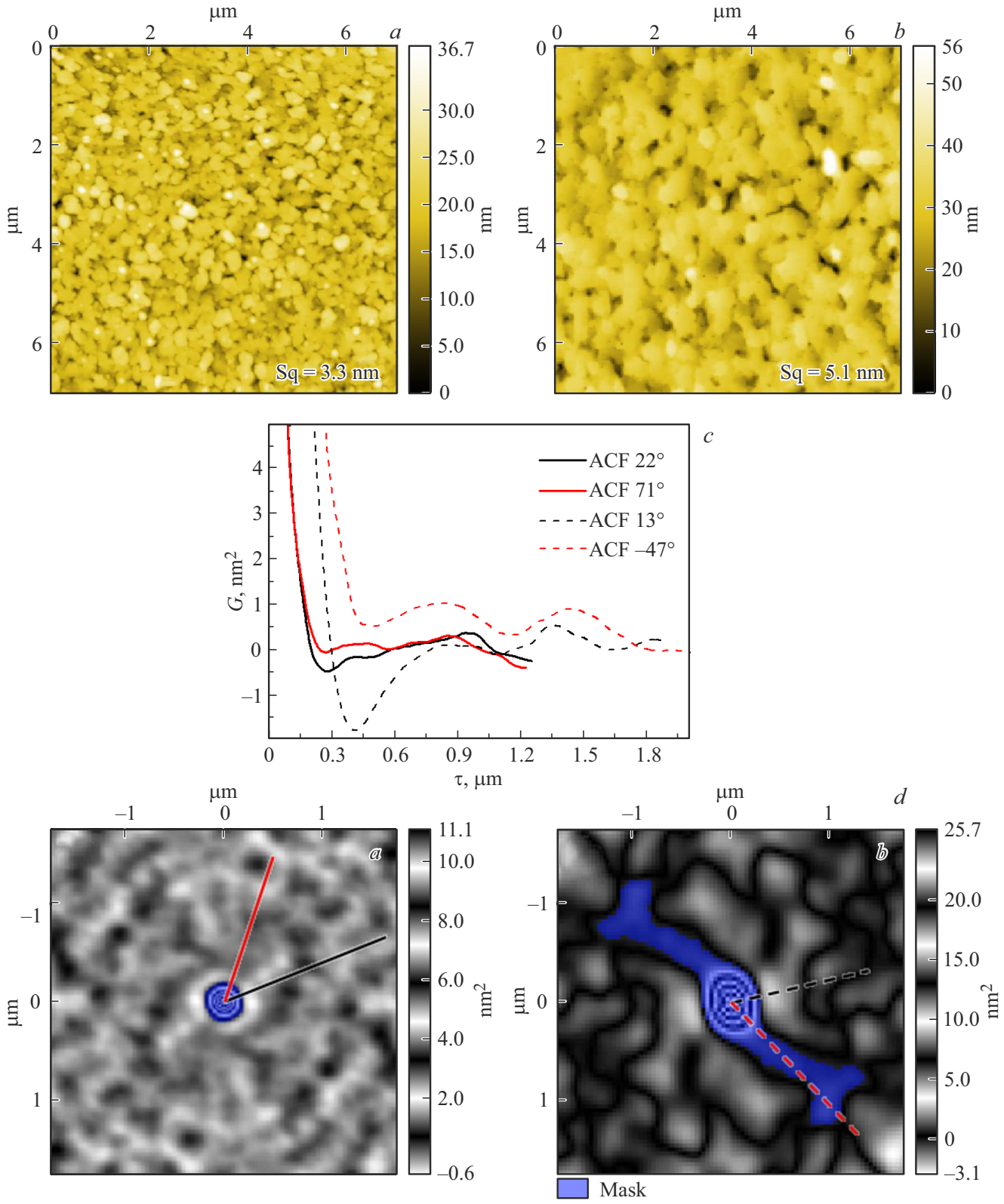

Figure 4. AFM data for Mn_5Ge_3 thin films grown *a* — directly on Si(111) silicon and *b* — on a preformed buffer layer. Sq — the RMS value of the irregularities height. *c* — ACF cross section, *d* — two-dimensional ACF; black and red lines mark the cross-section directions for the corresponding samples.

the autocorrelation length $S_{al}(\#a) = 118.0$ nm for the film obtained by maintaining the stoichiometric ratio of atom flux rates. The length of the slowest attenuation is 144.2 nm (red line along the direction 71°), which corresponds to the typical maximum size of the film elements.

The Frank–Van der Merwe mechanism (layered growth), typical for epitaxial films is implemented in the case of usage of a thin buffer layer Mn_xGe_y with a gradual transition to the stoichiometric composition of Mn_5Ge_3. The two-dimensional ACF for this case is S_{al} (#b) = 260.6 nm and is shown in Figure 4, *d* (#b). Pronounced anisotropy is observed, and the directions of the fastest and slowest attenuation (width and length of the terraces) can be clearly distinguished, which are 260.6 and 1608 nm (red dotted line along the direction −47°). In addition, the ACF allows calculating the surface texture coefficient (S_{tr}), which is defined as the ratio between the largest and smallest ACF attenuation distances and is for S_{tr} (#a) = 0.8184 and S_{tr} (#b) = 0.1621. It can be assumed that the strong anisotropy in the case of (#b) is associated with the growth of Mn_5Ge_3 terraces on silicon atomic steps, whereas the direct growth of Mn_5Ge_3 on silicon leads to the formation of crystallites of a more isotropic form.

4. Conclusion

Mn_5Ge_3 film was grown on Si(111) by molecular beam epitaxy with simultaneous deposition of Mn (growth rate 0.35 nm/min) and Ge (growth rate 0.32 nm/min). It was found using the RHEED data analysis that the formation of the cubic phase of MnSi silicide prevails at the initial stages of growth. The formation of the hexagonal phase Mn_5Ge_3 (*h*P16, $a = 0.71$ nm, $c = 0.50$ nm) begins in the thickness range of 2–7 nm which remains the only one when the thickness exceeds 10 nm. The analysis of atomic force microscopy data using a two-dimensional autocorrelation function showed that the direct growth of the Mn_5Ge_3 film on silicon corresponds to the Stranski-Krastanov mechanism unlike Mn_5Ge_3 films grown on a buffer layer [26], where layered epitaxial growth is realized with the formation of anisotropic terraces.

Acknowledgments

The authors thank the Krasnoyarsk Regional Research Equipment Sharing Center of the Federal Research Center Krasnoyarsk Science Center of the Siberian Branch of the Russian Academy of Sciences for the provided equipment.

Funding

This study was carried out as part of the state research assignment of the Kirensky Institute of Physics SB RAS.

Conflict of interest

The authors declare that they have no conflict of interest.

References

[1] I. Žutić, J. Fabian, S. Das Sarma. Rev. Mod. Phys. **76**, *2*, 323 (2004). https://doi.org/10.1103/RevModPhys.76.323
[2] A. Hirohata, K. Yamada, Y. Nakatani, I.-L. Prejbeanu, B. Diény, P. Pirro, B. Hillebrands. J. Magn. Magn. Mater. **509**, 166711 (2020). https://doi.org/10.1016/j.jmmm.2020.166711
[3] R. Jansen. Nature Mater. **11**, *5*, 400 (2012). https://doi.org/10.1038/nmat3293
[4] V.V. Ustinov, I.A. Yasyulevich, N.G. Bebenin. Phys. Met. Metallogr. **124**, *14*, 1745 (2023).
[5] N.G. Bebenin. JETP Lett. **118**, *5*, 336 (2023).
[6] L.A. Fomin, I.V. Malikov, V.A. Berezin. J. Surf. Invest.: X-Ray, Synchrotron Neutron Tech. **16**, *4*, 448 (2022).
[7] V.V. Marchenkov, V.Y. Irkhin. Phys. Metals Metallogr. **122**, *12*, 1133 (2021).
[8] A.S. Samardak, A.G. Kolesnikov, A.V. Davydenko, M.E. Stebliі, A.V. Ognev. Phys. Metals Metallogr. **123**, *3*, 238 (2022).
[9] V.D. Buchelnikov, D.R. Baigutlin, V.V. Sokolovskiy, O.N. Miroshkina. Phys. Metals Metallogr. **124**, *2*, 118 (2023).
[10] A.S. Tarasov, I.A. Tarasov, I.A. Yakovlev, M.V. Rautskii, I.A. Bondarev, A.V. Lukyanenko, M.S. Platunov, M.N. Volochaev, D.D. Efimov, A.Yu. Goikhman, B.A. Belyaev, F.A. Baron, L.V. Shanidze, M. Farle, S.N. Varnakov, S.G. Ovchinnikov, N.V. Volkov. Nanomater. **12**, *1*, 131 (2022). https://doi.org/10.3390/nano12010131
[11] A. Spiesser, I. Slipukhina, M.-T. Dau, E. Arras, V.L. Thanh, L. Michez, P. Pochet, H. Saito, S. Yuasa, M. Jamet, J. Derrien. Phys. Rev. B **84**, *16*, 165203 (2011). https://doi.org/10.1103/PhysRevB.84.165203
[12] Y. Kim, K.H. Kang, J.H. Kim, E.J. Kim, K. Choi, W.B. Han, H.-S. Kim, Y. Oh, C.S. Yoon. J. Alloys Compd **644**, 464 (2015). https://doi.org/10.1016/j.jallcom.2015.05.061
[13] Songlin, Dagula, O. Tegus, E. Brück, F.R. de Boer, K.H.J. Buschow. J. Alloys Compd **337**, *1–2*, 269 (2002).
[14] J. Tang, C.-Y. Wang, L.-T. Chang, Y. Fan, T. Nie, M. Chan, W. Jiang, Y.-T. Chen, H.-J. Yang, H.-Y. Tuan, L.-J. Chen, K.L. Wang. Nano Lett. **13**, *9*, 4036 (2013).
[15] R.P. Panguluri, C. Zeng, H.H. Weitering, J.M. Sullivan, S.C. Erwin, B. Nadgorny. Physica Status Solidi B **242**, *8*, R67 (2005). https://doi.org/10.1002/pssb.200510030
[16] A. Spiesser, H. Saito, R. Jansen, S. Yuasa, K. Ando. Phys. Rev. B **90**, *20*, 205213 (2014). https://doi.org/10.1103/PhysRevB.90.205213
[17] A. Berche, J.C. Tedenac, P. Jund. Intermetallics **47**, 23 (2014). https://doi.org/10.1016/j.intermet.2013.12.009
[18] R.C. de Oliveira, D. Demaille, N. Casaretto, Y.J. Zheng, M. Marangolo, D.H. Mosca, J. Varalda. J. Magn. Magn. Mater. **539**, 168325 (2021). https://doi.org/10.1016/j.jmmm.2021.168325
[19] D.D. Dung, D. Odkhuu, L.T. Vinh, S.C. Hong, S. Cho. J. Appl Phys. **114**, *7*, 073906 (2013). https://doi.org/10.1063/1.4817372
[20] M. Petit, L. Michez, C.-E. Dutoit, S. Bertaina, V.O. Dolocan, V. Heresanu, M. Stoffel, V.L. Thanh. Thin Solid Films **589**, 427 (2015).
[21] A. Spiesser, V.L. Thanh, S. Bertaina, L.A. Michez. Appl. Phys. Lett. **99**, *12*, 121904 (2011).
[22] B.T. Yasasun, A.C. Önel, I.G. Aykac, M.A. Gulgun, L.C. Arslan. J. Magn. Magn. Mater. **473**, 348 (2019).

[23] I. Yakovlev, I. Tarasov, A. Lukyanenko, M. Rautskii, L. Solovyov, A. Sukhachev, M. Volochaev, D. Efimov, A. Goikhman, I. Bondarev, S. Varnakov, S. Ovchinnikov, N. Volkov, A. Tarasov. Nanomater. **12**, *24*, 4365 (2022). https://doi.org/10.3390/nano12244365
[24] A.S. Tarasov, S.V. Komogortsev, A.V. Lukyanenko, I.A. Yakovlev, I.A. Tarasov, A.L. Sukhachev, M.V. Rautskii, L.A. Solovyov, T.A. Andryushchenko, I.A. Bondarev, S.N. Varnakov, N.V. Volkov. J. Mater. Sci. **59**, *21*, 9423 (2024). https://doi.org/10.1007/s10853-024-09755-6
[25] M.V. Rautskii, A.V. Lukyanenko, S.V. Komogortsev, I.A. Sobolev, L.V. Shanidze, I.A. Bondarev, M.A. Bondarev, E.V. Eremin, I.A. Yakovlev, A.L. Sukhachev, M.S. Molokeev, L.A. Solovjov, S.N. Varnakov, S.G. Ovchinnikov, N.V. Volkov, A.S. Tarasov. Physics of Metals and Metallography, 2024, Vol. 125, No. 12, pp. 1327–1336. DOI: 10.1134/S0031918X24601975
[26] A.S. Tarasov, A.V. Lukyanenko, I.A. Tarasov, I.A. Bondarev, T.E. Smolyarova, N.N. Kosyrev, V.A. Komarov, I.A. Yakovlev, M.N. Volochaev, L.A. Solovyov, A.A. Shemukhin, S.N. Varnakov, S.G. Ovchinnikov, G.S. Patrin, N.V. Volkov. Thin Solid Films **642**, 20 (2017). https://doi.org/10.1016/j.tsf.2017.09.025
[27] I.A. Tarasov, M.A. Visotin, T.V. Kuznetzova, A.S. Aleksandrovsky, L.A. Solovyov, A.A. Kuzubov, K.M. Nikolaeva, A.S. Fedorov, A.S. Tarasov, F.N. Tomilin, M.N. Volochaev, I.A. Yakovlev, T.E. Smolyarova, A.A. Ivanenko, V.I. Pryahina, A.A. Esin, Y.M. Yarmoshenko, V.Ya. Shur, S.N. Varnakov, S.G. Ovchinnikov. J. Mater. Sci. **53**, *10*, 7571 (2018). https://doi.org/10.1007/s10853-018-2105-y
[28] A.S. Tarasov, A.V. Lukyanenko, I.A. Yakovlev, I.A. Tarasov, I.A. Bondarev, A.L. Sukhachev, L.V. Shanidze, D.A. Smolyakov, S.N. Varnakov, S.G. Ovchinnikov, N.V. Volkov. Bull. Russ. Acad. Sci.: Phys. **87**, *Suppl. 1*, S127 (2023).
[29] I.A. Yakovlev. State reg. software for computers 2018611121. A program for calculating electron diffraction patterns from a cubic crystal (2017).
[30] N.P. Lyakishev. Diagrammy sostoyaniya dvoynykh metallicheskikh sistem: spravochnik v 3 t. Mashinostroenie, M. (1997). (in Russian).
[31] A. Ichimiya, P.I. Cohen. Reflection high-energy electron diffraction. University Press, Cambridge, UK (2004). 353 p.
[32] D. Nečas, P. Klapetek. Ultramicroscopy **124**, 13 (2013). https://doi.org/10.1016/j.ultramic.2012.08.002

Translated by A.Akhtyamov